IOP Conf. Series: Materials Science and Engineering **418** (2018) 012118 doi:10.1088/1757-899X/418/1/012118

Experimental investigation on tube flaring with a rotating tool

E M Mamros and C P Nikhare*

Mechanical Engineering, The Pennsylvania State University, The Behrend College, Erie, PA 16563 USA

*corresponding author: cpn10@psu.edu

Abstract. As the automotive industry becomes increasingly competitive, manufacturers are striving to design the lightest, most fuel-efficient vehicles to capture the market. To achieve this mission, the material processing techniques used in vehicle manufacturing must be investigated further. One such critical technique is sheet metal forming, which creates parts that account for a large percentage of the total vehicle weight. Many of these sheet metal parts make up the structure of the vehicle and are constructed from thin-walled tubes. To manufacture these thin-walled tubes into the desired shape, one of the main techniques is tube forming which can expand or reduce the tubes' diameters to the desired dimension. One specific tube forming technique is the flaring process which is typically performed at the tube end. In this paper, the tool rotation at its flaring axis was considered. The analysis of the expansion ratio, strain path, and failure limit was also performed along with experimentation. Frictional effects were considered. It was observed that varying the rotational speed of the flaring tool influenced the ability of the tube to flare. The expansion ratio can be maximized with a decreased amount of friction, a lower rotational speed of the flaring tool, and with an increase in tool velocity.

1. Introduction

In a world becoming increasingly concerned with the environment, air pollution from emissions and travel efficiency are major concerns for manufacturers in the automotive industries. In order to comply with the green initiative, companies are taking steps to make vehicles lighter and more fuel-efficient while maintaining quality and safety standards [1]. The heavier the vehicle, the lower the fuel-efficiency and thus the higher the gasoline consumption and pollution level. One approach to work towards these goals is to further investigate the material processing techniques involved in the manufacture of vehicles. Some manufacturers are considering automation in their plants to simultaneously increase the efficiency, productivity, and quality of operations [2].

A large percentage of an automobile's weight is accounted for by sheet metal parts created from thin-walled tubes. In order to create the tubular parts, the tubes first must undergo a manufacturing process called tube forming. Tube forming is a technique used to either increase or decrease the diameter of the tubes into the appropriate dimension for the subsequent part. A common forming technique is the flaring process usually performed at the end of the tube [3]. Forming is typically performed to either join the tube with other tubes or parts, create a connection between the joint and jointing parts, to adjust tube support, or to make a pathway for fluid flow [4].

Tube flaring is a process that requires extremely complex metal flows. Several factors that play an important role in tube flaring practice are friction, temperature, and angle of the flaring tool [5-6]. The conventional method of tube flaring involves using displacement along the axial direction to insert a conical punch into a tube of the same diameter forcing the tube's diameter to expand [7].

Content from this work may be used under the terms of the Creative Commons Attribution 3.0 licence. Any further distribution of this work must maintain attribution to the author(s) and the title of the work, journal citation and DOI.
Published under licence by IOP Publishing Ltd

The stroke is related to the flaring ratio and tube end downward depth ratio by values that are usually determined experimentally. The flaring ratio is the ratio between the original diameter of the tube and the flared diameter of the tube [8]. Flaring a tube until failure is known as the flaring test and is commonly used to determine the circumferential ductility and material behavior of the tube. The flaring ability of the tube is restricted by two factors: the loss of overall stability due to elasto-plastic buckling in the non-formed part of the tube and loss of material stability from necking followed by fracture in the conical edge of the tube [9]. The specimen length dictates which instability will cause the tube to fail, with longer tubes tending to buckle and shorter ones tending to neck and crack [9]. Incorporating rotation into the flaring process significantly decreases the press load on the tube and requires a lesser power input than conventional flaring [11].

Several studies have attempted to perform numerical and finite element analysis of the flaring process, but these simulations are often difficult to create and run. The most challenging aspects of creating these simulations are being able to model the correct wall thickness variations after forming and the contact of the tool and the tube while forming [12].

In the past, testing has been performed using a conventional flaring method while the tube was spinning or electromagnetic forming which is expensive and resource-intensive [13]. Electromagnetic forming involves a number of parameters that can be adjusted to alter the flaring of the tube: charge energy of the condenser bank, the coil protector's electrical properties, tube length, tube positioning, and degree of coil taper [14]. Another study considered the effects of using the conventional method of flaring with a series of punches, starting with a slightly elliptical tool followed by a "sharp" elliptical punch [15].

In this study, a new approach to the flaring process was taken using a spinning conical steel tool with varying rotational speeds to perform the flaring procedure on a static tube. Experiments were performed at 0 RPM (conventional flaring), 100 RPM, and 200 RPM. One additional set of experiments was performed at 100 RPM with a motor oil coolant to investigate the effects of friction from the metal-metal contact. Each set of experiments involving the rotating tool were compared to the conventional flaring technique (no spinning).

2. Methodology

2.1. Tensile Test

The forming of 4130 alloy steel tubes with 19.05 mm (0.75 in) outer diameter and a wall thickness of 0.711mm (0.028 in) was investigated in this study. To create the specimens for the tensile test, dog bones were machined in the longitudinal direction using computer numerical control (CNC) milling, and their geometry is shown in Figure 1.

Three dog bone specimens were tested at room temperature on the MTS machine with 5mm/min pulling speed using the experimental setup shown in Figure 1.

2.2. Tube Flaring

The cylindrical tube specimens were cut in lengths of 70 mm (2.75 in) to perform the tube flaring experiments. The tool with a cone angle of 30° was made up of as-received D2 steel with a hardness of 25HRC. The bottom diameter of the tool was 10.2mm (0.4 in) as shown in Figure 1. The tool was redressed to these dimensions following each experiment to maintain the geometric consistency. Three sets of experiments were performed: 0, 100, and 200 RPM, each at a constant feed rate of 5 mm/min (0.2 in/min). Three specimens were tested for each set of experiments to ensure repeatability. Each test ended when a crack was observed. Further analysis of force-displacement data provided the tool displacement at failure.

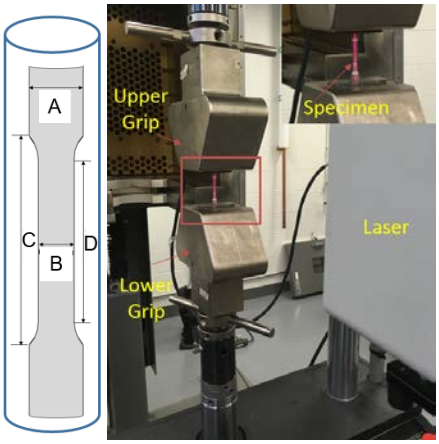


Figure 1. Dog-bone specimen geometry (specimen dimensions: A = 9.5 mm; B = 6.35 mm; C = 38.1 mm; and D = 29.7 mm) [16] (left); and tensile test setup with close-up on MTS Machine (right)

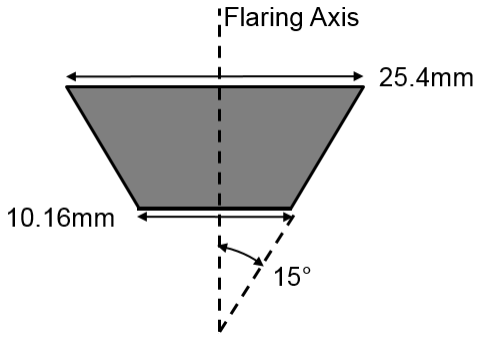
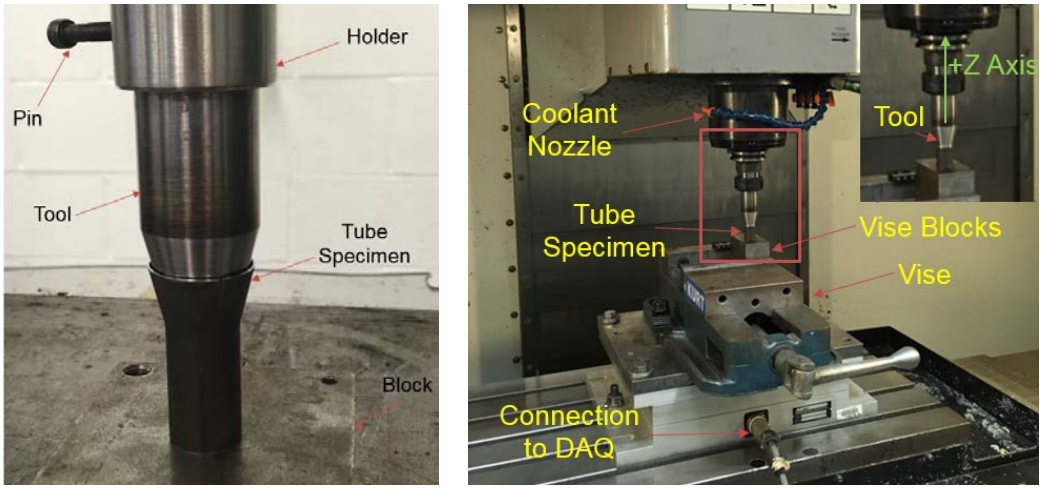


Figure 2. Conical flaring tool

2.2.1. Conventional Tube Flaring. The tubes were flared with the conical tool using the conventional method (without rotation) on the Tinius-Olsen 120 kip machine. The specimens were flared until failure, and the force in the axial direction was recorded. The specimens were placed on the bottom platen, and the tool was inserted into the crosshead as shown in Figure 3a. A tool speed of 5mm/min was used.

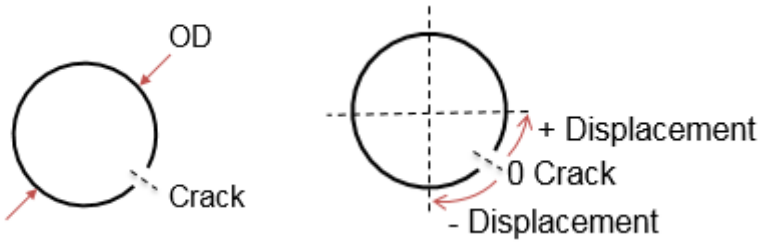


(a) (b)

Figure 3. Experimental setup for flaring on: (a) Tinius-Olsen (for conventional flaring), (b) CNC (for rotational flaring)

2.2.2. Tube Flaring with Rotating Tool. All flaring experiments involving the rotation of the tool about the flaring axis were performed on the HAAS CNC machine at a constant feed rate of 5mm/min as shown in Figure 3b. Tubes were flared at a tool rotation rate of 100 and 200RPM, and the AMTI data acquisition device at a sampling rate of 1000Hz was used for each experiment to record the force in the axial direction.

2.3. Profile Measurement
Following each set of experiments, the flared end of each tube was laid flat on grid paper, and the diameter was traced. A Vernier caliper was used to measure the flared outer diameter (OD). The traced images were then digitally converted and an example is shown in Figure 4a.



(a) (b)

Figure 4. (a) Profile measurement; (b) Thickness distribution measurement

2.4. Thickness Measurement
The thickness distribution of the top quarter edge of each tube was measured using a Vernier caliper with 0.025mm (0.001inch) accuracy. The failure edge was designated as the "0" location as shown in Figure 4b, and thickness measurements were taken in each direction (positive and negative) of the "0" location.

2.5. Microstructure
A section of the tube specimen near the failure region was mounted for microscopy and the microstructure at the failure site was examined under a scanning electron microscope (SEM) for each of the following specimens: as received, conventional tube flaring, rotational tube flaring at 100, and 200 RPM.

3. Results and Discussion

3.1. Tensile Test
Figure 5 displays the true stress-strain curve that resulted from the tensile experimental data being fitted with the Holloman-Ludwik equation (Power Law) given in Equation 1. The mechanical properties can be found in Table 1.

$$\sigma = K \cdot \varepsilon^{n} \quad (1)$$

3.2. Tube Flaring
It was found that the axial force decreased as the rotational speed of the flaring tool was increased. This finding shows that as the speed of the flaring tool increases, the probability of the tube failing via buckling decreases.

The amount of friction created and the rise in temperature of the tube specimen were directly related to the change in rotational speed of the flaring tool. At higher rotational speeds, the flaring tool generated a larger amount of friction and heat experienced by the tube specimen.

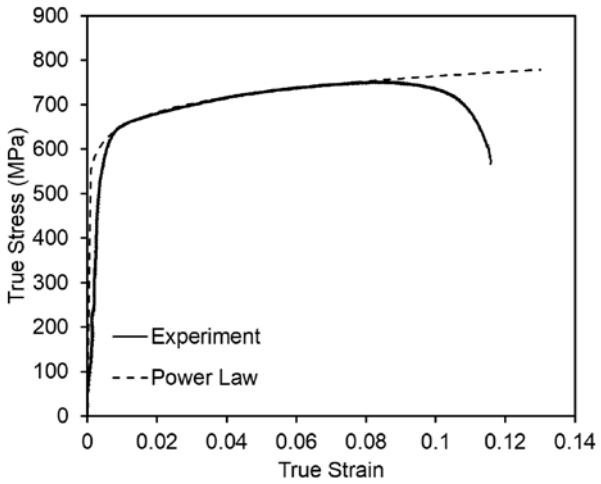
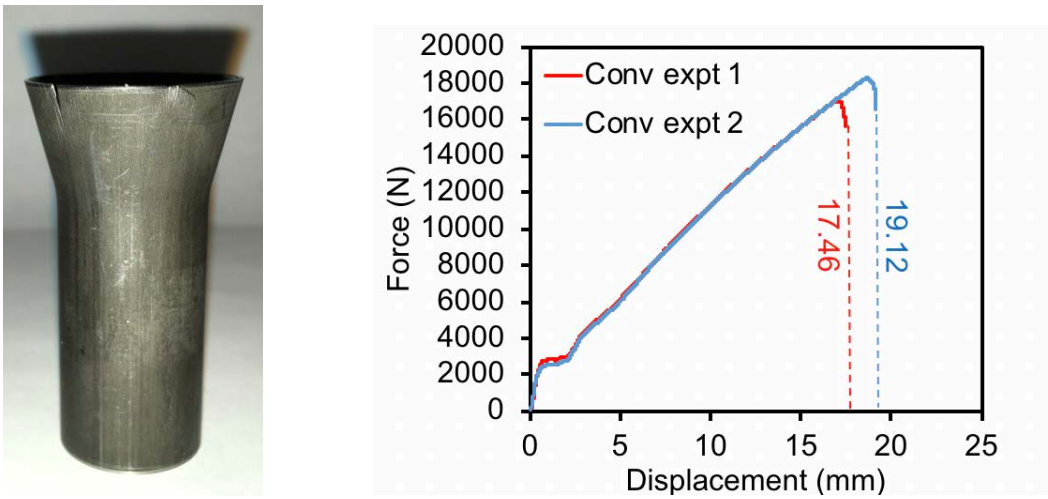


Figure 5. Tensile true stress-strain curve for 4130 alloy steel

Table 1. Mechanical properties of 4130 alloy steel

Yield Stress (MPa)	Tensile Stress (MPa)	Elongation (%)	Strength Coefficient "K" (MPa)	Strain Hardening Exponent "n"
501	794	313	898	0.07

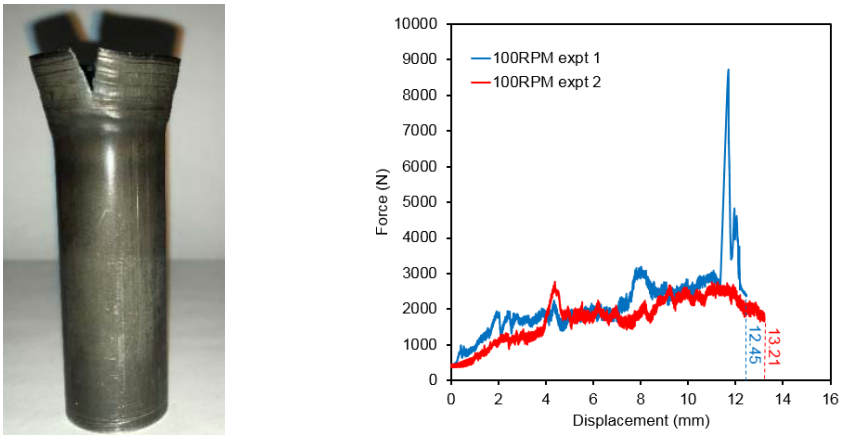
3.2.1. Conventional Tube Flaring.
As shown in Figure 6, the tube specimens that were flared conventionally experienced approximately 17000 N or more of force before failure. These specimens also allowed the tool to displace approximately 17 mm or more before failure.



(a) (b)

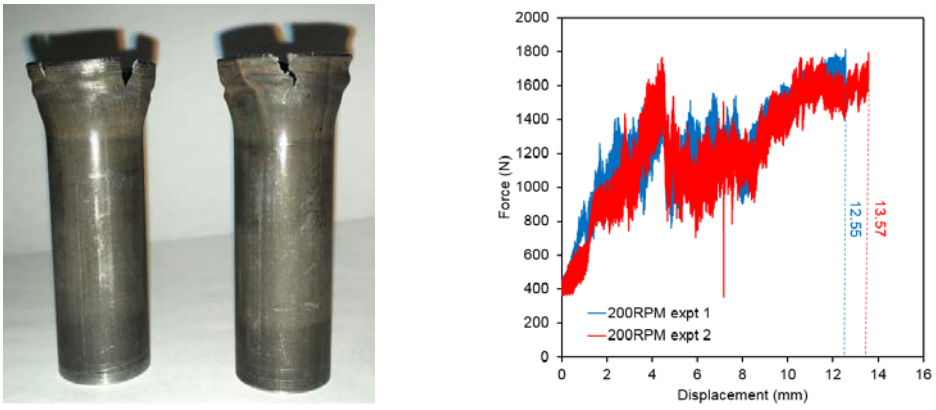
Figure 6. Conventional flaring: (a) Specimen, (b) Force-displacement curve

3.2.2. Tube Flaring with Rotating Tool.
As shown in Figure 7, the specimens flared at 100 RPM experienced relatively low forces of approximately 3000 N or less during the entire flaring with rotation process. The tool displaced 12.45 mm and 13.21 mm before failure as shown in Figure 7b.



(a) (b)

Figure 7. Flared at 100 RPM: (a) Specimen, (b) Force-displacement curve



(a) (b)

Figure 8. Flared at 200 RPM: (a) Specimens, (b) Force-displacement curve

As shown in Figure 8, the specimens flared at 200 RPM were able to be flared to the extent that the tool displaced 12.55mm and 13.57mm. These specimens experienced approximately 1800 N of force or less throughout the entire flaring process before failure.

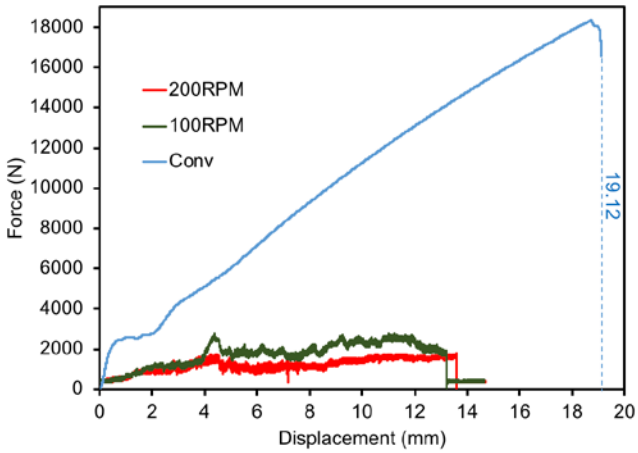


Figure 9. Force-displacement for 200 RPM, 100 RPM, and conventional experiments

As shown in Figure 9, the conventionally flared specimens experience a much larger force in the axial direction than the 100 RPM and 200 RPM specimens. Adding rotation to the flaring tool greatly decreased the force experienced by the specimen in the axial direction and decreased the risk of buckling. Also, the 200 RPM specimens experienced less force than the 100 RPM specimens. Following this trend, the faster the rotation of the flaring tool, the less force experienced by the specimen being flared and therefore the more the tube can be flared before failure provided that the temperature gradient helps the material to deform rather than to fail. To increase flaring, the tool must be able to displace a further depth into the specimen. The 200 RPM specimens allowed the tool to displace approximately 1mm further than the 100 RPM specimens allowed.

3.3. Profile Measurement

As shown in Figure 10, the flared tube specimens exhibit symmetry with the largest fracture region as a center point. The conventionally flared specimens have the largest outer diameter after flaring, but the 100 RPM and 200 RPM specimens also show a significant enlargement of the diameter when compared with as received specimens.

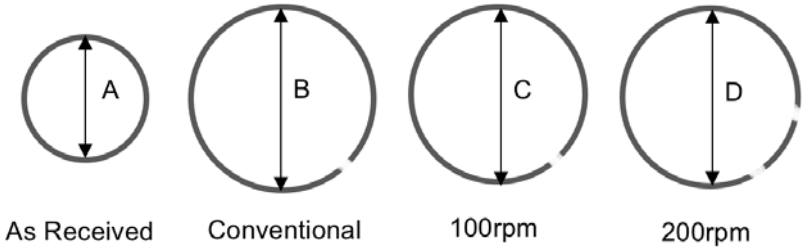


Figure 10. Flared tube specimen profiles

Table 2. Profile measurements

Specimen	Outer Diameter (mm)	% Expansion (%)
As Received	A = 17.93	--
Conventional (0 RPM)	B = 26.82	49.55
100 RPM	C = 25.78	43.68
200 RPM	D = 25.91	44.44

As shown in Table 2, the 100 RPM and 200 RPM specimen percentage expansions are within 6% of the conventional specimen (50%). The 100 RPM and 200 RPM specimens have very similar outer diameter measurements after flaring. The conventionally flared specimen showed the largest outer diameter of 26.82 mm.

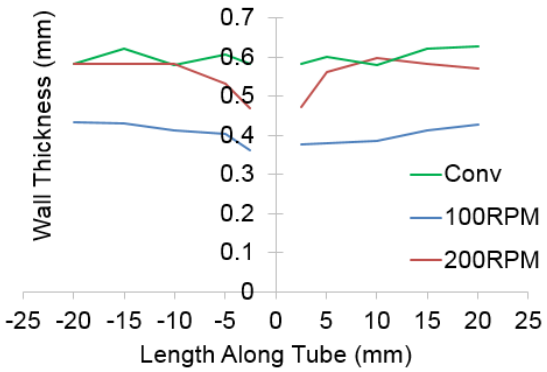


Figure 11. Thickness distribution of top quarter edge of specimens from failure location

3.4. Thickness Distribution

Figure 11 shows the thickness distribution measured along the top quarter edge of 100 RPM, conventional, and 200 RPM specimens from the failure location. The blank space represent the failure region, where the tube is split and material is not available to measure and record a thickness value.

Considering the failure region as the center point, the tube thickness is symmetrical on the left- and right-hand sides. As shown in Figure 11, the conventional tube specimens and 200 RPM tube specimens had very similar wall thicknesses around the failure region. The 100 RPM tube specimens had a slightly thinner wall thickness around the failure region. The conventional specimens showed localized thinning near the failure region.

3.5. Microstructure

Figure 12 shows the microstructure of the as-received tube from the manufacturer with isotropic, equiaxed grains. As shown in Figure 13a, there is no difference in microstructure found between the material from tool-side and the outside of the conventional tube flaring specimen. Conventional flaring does not appear to have any effect on the microstructure. As shown in Figures 13b and 13c, sliding was found on the tool-side with finer, more aligned grains, and coarser grains were found on the outside (tool not touching) microstructure. The material appears to flow more on the tool-side than on the outside. The rotation of the tool considerably alters the microstructure on the inside of the tube due to the tool-to-tube contact while the outside of the tube maintains the as-received microstructure.

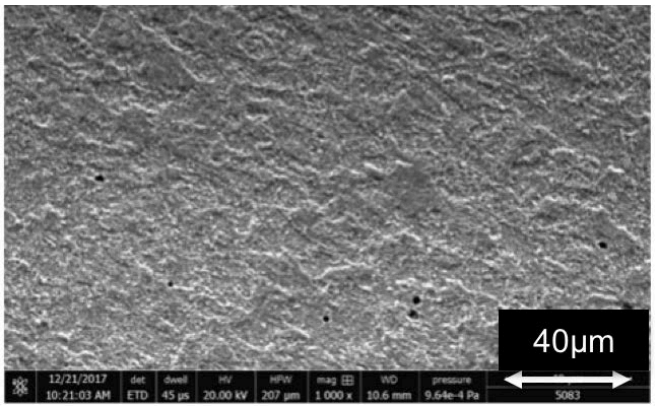
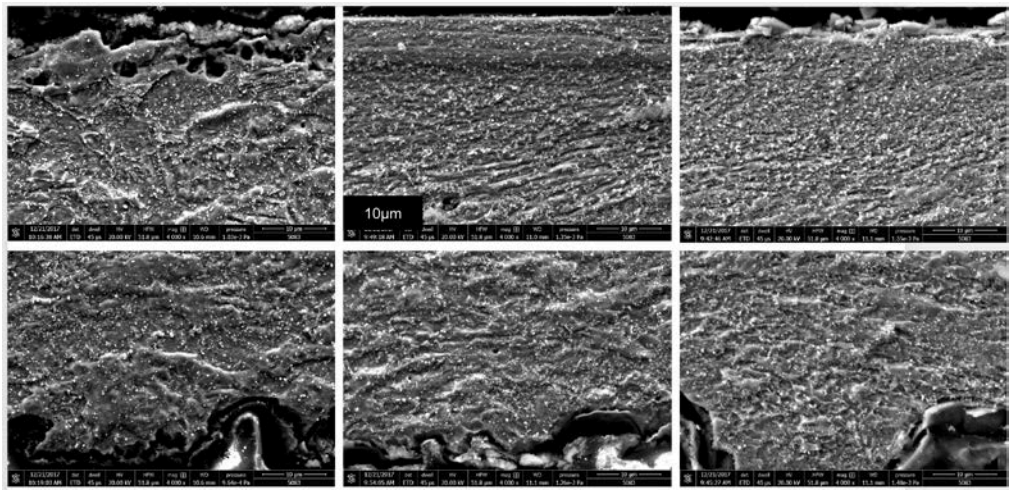


Figure 12. Microstructure of As Received specimen at 1000x magnification.



(a) (b) (c)

Figure 13. Tool-side (top row) and outside (bottom row) microstructure for specimens: (a) conventional, (b) 100RPM, (c) 200RPM at 4000x Magnification.

3.6. Element Mechanics

Figure 14 shows the stress states and associated principal stresses for different flaring scenarios. In each scenario, σ_t represents the thickness stress, σ_c represents the circumferential stress, and τ represents the shear stress. Also, σ_1 is always greater than σ_2 which is always greater than σ_3.

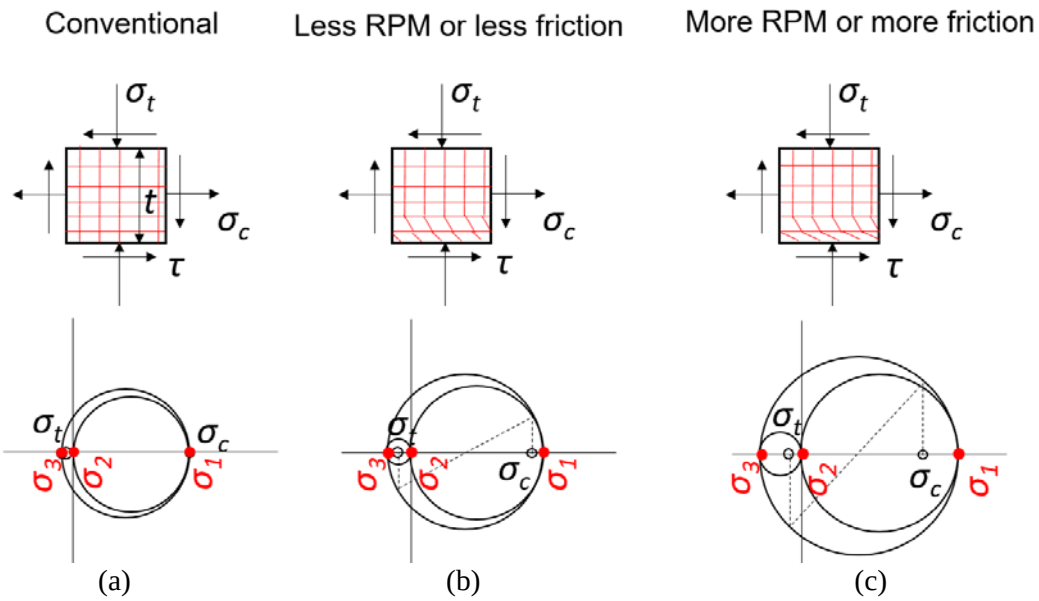


Figure 14. Stress differential elements and Mohr's circles for: (a) Conventional flaring, (b) Flaring with less RPM or less friction, (c) Flaring with more RPM or more friction.

During conventional flaring, the elements in the tube inner diameter edge do not see any shear stresses in the circumferential direction since the tool is not spinning as observed in Figure 13a. In rotational flaring, when the friction generated is minimum either by lower RPM or by the usage of high temperature lubricant to reduce the friction, the shear stress generation would be minimum and thus the material sliding can be seen less. This shear stress increases the diameter of Mohr's circle and thus increases the values of the principal stresses in comparison to the conventionally flared circle. In the case of higher friction generation (i.e., more RPM), the shear stress would be higher and material would slide more. This higher generated shear stress would significantly increase the Mohr's circle and thus the principal stress would be even higher. In both case, it seems that the material would lead to failure faster based on the conventional forming limit curve. However if the material softening is considered due to friction induced heat, then the overall stress value would be less and the rotational flaring would delay the failure with higher formability. Higher formability can also be achieved due to higher deformation in thickness which would raise the through thickness stress, which is generally ignored in forming limit curve. This factor cannot be ignored while comparing the strain path on forming limit curve. Due to significant stresses in thickness direction the forming limit will rise and more deformation can be achieved in rotational flaring.

4. Conclusions and Future Work

The flaring operation with rotational tool was studied in this paper. For this the tubes were flared with different tool rotational speeds and compared with the conventional flaring. Through investigation, it was found that there are three main parameters affecting the temperature of the tube and therefore the ability of the tube to flare: friction, rotational speed of the flaring tool, and the tool velocity. The friction created by tool-to-tube contact can be varied by using an appropriate lubricant or changing the material of the tool. To optimize the ability of the tube to flare, the friction between the tool and the specimen should be reduced. The rotational speed of the tool needs to be adjusted such that the enough

heat generation due to friction can be achieved which will help material to flow plastically rather than fail due to liquidity. It was observed that the more uniform thickness distribution was achieved with lower RPM. This indicates that the higher formability could have been achieved. The tool velocity also affects the ability of the tube to flare and depends on the rotational speed of the tool. The slower the rotational speed of the tool, the further the depth the tool is able to travel and flare the tube, again link with heat generation due to friction.

To increase the flaring of a tube, the condition needs to obtain where the tube material hold its strength but also gain plastic flow-ability. As hypothesized, a tube that is flared at a lower RPM or that has a reduced amount of friction during flaring will have lower stresses than a tube that is flared at a higher RPM or that has an increased amount of friction present. However, a third direction i.e., thickness strain will be dominant which cannot be ignored while comparing the strain path and may result in higher limits. To prove this concept, future investigation will focus on running more experiments with different tool speeds and using a high temperature lubricant.

Acknowledgements
The authors would like to acknowledge the funding and support of undergraduate research projects from Penn State Behrend. The authors would also like to thank technician Mr. Glenn Craig for his assistance with setting the experiments.

References

[1] Gipiela M L, Amauri V, Nikhare C, and Marcondes P V P 2017 *IOP Conference Series: Materials Science and Engineering* 164(1) 012009
[2] Almeida B P P, Alves M L, Rosa P A R 2006 *International Journal of Machine Tools and Manufacture* **46**(12) 1643
[3] Seibert H, Petrut L, and Nikhare C P 2017 *Journal of Manufacturing and Materials Processing* **1**(2)
[4] Huang Y M 2009 *The International Journal of Advanced Manufacturing Technology* **43**(11) 1167
[5] Huang Y 2004 *The International Journal of Advanced Manufacturing Technology*, **24**(1) 91
[6] Zhao X, Xu W, Chen Y, 2017 *The International Journal of Advanced Manufacturing Technology* **88**(5) 1983
[7] Huang Y 2001 *The International Journal of Advanced Manufacturing Technology* **18**(6) 390
[8] Lu Y 2004 *Finite Elements in Analysis and Design* **40**(3) 305
[9] Mirzai M A, Manabe K, and Mabuchi T 2008 *Journal of Materials Processing Technology* **201**(1) 214
[10] Daxner T, Rammerstorfer F G, and Fischer F D 2005 *Computer Methods in Applied Mechanics and Engineering* **194**(21) 2591
[11] Tamang S, Bylya O, Ward M 2017 *AIP Conference Proceedings* **1896**(1) 050002
[12] Fischer F D. Rammerstorfer F G, and Daxner T 2006 *International Journal of Mechanical Sciences* **48**(11) 1246
[13] Khalil Hazawi A R, Abdel-Magied R, and Elsheikh M N 2017 *The International Journal of Advanced Manufacturing Technology* **92**(1) 157
[14] Murata M, and Suzuki H 1990 *Journal of Materials Processing Technology* **22**(1) 75
[15] Nikhare C P, Korkolis Y P, and Kinsey B L 2015 *Journal of Manufacturing Science and Engineering* **137**(5) 1
[16] Pier B, Nikhare C 2018 *Proc. of the ASME 2018 International Manufacturing Science and Engineering Conference* (accepted)